

Dynamical Downscaling of Seasonal Climate Prediction over Nordeste Brazil with ECHAM3 and NCEP's Regional Spectral Models at IRI



Paulo Nobre,* Antonio D. Moura, and Liqiang Sun
International Research Institute for Climate Prediction,
Lamont-Doherty Earth Observatory of Columbia University, Palisades, New York

ABSTRACT

This study presents an evaluation of a seasonal climate forecast done with the International Research Institute for Climate Prediction (IRI) dynamical forecast system (regional model nested into a general circulation model) over northern South America for January–April 1999, encompassing the rainy season over Brazil's Nordeste. The one-way nesting is one in two tiers: first the NCEP's Regional Spectral Model (RSM) runs with an 80-km grid mesh forced by the ECHAM3 atmospheric general circulation model (AGCM) outputs; then the RSM runs with a finer grid mesh (20 km) forced by the forecasts generated by the RSM-80. An ensemble of three realizations is done. Lower boundary conditions over the oceans for both ECHAM and RSM model runs are sea surface temperature forecasts over the tropical oceans. Soil moisture is initialized by ECHAM's inputs.

The rainfall forecasts generated by the regional model are compared with those of the AGCM and observations. It is shown that the regional model at 80-km resolution improves upon the AGCM rainfall forecast, reducing both seasonal bias and root-mean-square error. On the other hand, the RSM-20 forecasts presented larger errors, with spatial patterns that resemble those of local topography. The better forecast of the position and width of the intertropical convergence zone (ITCZ) over the tropical Atlantic by the RSM-80 model is one of the principal reasons for better-forecast scores of the RSM-80 relative to the AGCM. The regional model improved the spatial as well as the temporal details of rainfall distribution, and also presenting the minimum spread among the ensemble members. The statistics of synoptic-scale weather variability on seasonal timescales were best forecast with the regional 80-km model over the Nordeste. The possibility of forecasting the frequency distribution of dry and wet spells within the rainy season is encouraging.

1. Introduction

Atmospheric general circulation models (AGCMs) are capable of simulating some aspects of large-scale patterns of seasonal rainfall over the Tropics with

surprisingly high accuracy (Mehoso et al. 1990). To a great extent, this is due to the controlling effect of tropical sea surface temperature (SST) on a time-averaged (months and longer) atmospheric phenomena in the Tropics (Shukla 1981). So, the feasibility of skillful, long-lead seasonal mean climate forecasts for the Tropics depends on the availability of skillful SST forecasts over the tropical oceans (Ward and Folland 1991). However, the applicability of such seasonal forecasts to hydrology and agriculture, for example, is strongly tied to finer time/space resolution of the forecasts than that of a typical AGCM. The development of statistical and dynamical ocean models during the last two decades has provided skillful prediction tools for long-lead tropical SST forecasts. For example, see the *Experimental Long-Lead Fore-*

*On leave of absence from Centro de Previsão de Tempo e Estudos Climáticos, Instituto Nacional de Pesquisas Espaciais, Cachoeira Paulista, São Paulo, Brazil.

Corresponding author address: Dr. Paulo Nobre, International Research Institute for Climate Prediction, Lamont-Doherty Earth Observatory of Columbia University, 61 Route 9W, IRI Monell Bldg., Palisades, NY 10964-8000.

E-mail: pnobre@cptec.inpe.br

In final form 11 May 2001.

©2001 American Meteorological Society

cast Bulletin (Kirtman 1999). Presently, long-lead SST anomaly forecasts are available on a regular basis not only for the tropical Pacific Ocean (Zebiak and Cane 1987) but also for the Atlantic (Repelli and Nobre 2001) and the Indian Oceans (Mason et al. 1999). These SST forecasts are currently used in a two-tiered forecasting approach to generate seasonal rainfall and temperature forecasts globally (e.g., see <http://iri.ldeo.columbia.edu/climate/forecasts/>).

However, due to their coarse spatial and temporal resolutions, such seasonal climate forecasts are of limited practical value for decision makers. Coupling the outputs of seasonal climate forecasts with distributed hydrological models (Galvão et al. 1999), or crop management algorithms, puts stringent requirements on the temporal and horizontal scales of the meteorological forecasts. Thus, it is of interest to evaluate to what extent the statistics of higher-frequency–smaller-scale rainfall distribution is predictable over Nordeste Brazil, a region where seasonal mean interannual rainfall variability is itself highly predictable.

Due to computational constraints, AGCMs are typically run at a resolution far too coarse to provide information (e.g., precipitation, temperature) at spatial and temporal resolutions useful for direct application. One remedy for this is the adoption of a dynamical downscaling approach. A high-resolution limited-area model is run for the region of interest, forced by the large-scale circulation prescribed from a lower-resolution AGCM. Several studies already examined this approach for particular areas such as the Asian monsoon region (Ji and Vernekar 1997) and North America (Fennessy and Shukla 1998). These simulation experiments used the National Centers for Environmental Prediction's (NCEP) Eta regional model ensembles with an 80-km horizontal grid nested on the Center for Ocean–Land–Atmosphere Studies AGCM at a horizontal truncation of R40. Their regional model nesting strategy resulted in simulated precipitation and circulation patterns that resembled observations better than did the corresponding AGCM simulated patterns. Dynamical downscaling has also been coupled with hydrological models. Leung et al. (1999) used the Pacific Northwest National Laboratory Regional Climate Model to downscale NCEP Medium-Range-Forecast (MFR) model simulations during the warm phases of ENSO. In their study, the regional model improved the rainfall simulations produced by the AGCM.

The present work is an actual dynamical downscaling forecast experiment (using actual SST forecast

fields as oceanic lower-boundary conditions). The regional model of choice is an anomaly model, which uses the AGCM outputs over the entire regional domain as base fields. Additionally, two-step nesting is done to investigate whether the forecast rainfall fields resulting from the first nesting step of the regional model could be further improved. The study addresses the northern portion of South America during the period January–April 1999, which is the rainy season over the Brazilian Nordeste. Section 2 describes the methodology and data used; results and discussion are presented in section 3, followed by conclusions in section 4.

2. Methodology and data

The regional climate forecast system implemented at the IRI consists of the hydrostatic version of NCEP Regional Spectral Model (RSM) (Juang and Kanamitsu 1994) nested in the Max Planck Institute ECHAM3 AGCM. The one-way nesting of the regional model into the global model was done in a way that is different from conventional methods, which use global results along the lateral boundary zone only. The perturbation nesting method used here allows the global model to be used over the entire regional domain, not just in the lateral boundary zone. The dependent variables in the regional domain are defined as a summation of perturbation and base. The base is a time-dependent prediction from the global model. All other features that cannot be predicted by the global model but can be resolved and predicted by the regional model in the regional domain are defined as perturbations. Nesting is done in such a way that the perturbation may be nonzero inside the regional domain but only zero outside of it. The perturbation computations in the regional domain include a semi-implicit time scheme, time filtering, initialization, and implicit horizontal diffusion.

Several test simulations were performed to determine the appropriate horizontal resolution and size of the computational domain. The size and specific geographic location of the computational domain has to be specified such that the terrain is smooth and there is no strong convection in the lateral buffer zone. We found that model outputs are sensitive to the model resolution and the location of lateral boundaries. The current domain (Fig. 1) represents a compromise between the requirement for high model resolution and the available computational resources. The nesting is

done in two steps. 1) The regional model with $80 \text{ km} \times 80 \text{ km}$ resolution in the horizontal (covering the region 23°S – 16°N , 85° – 25°W) and 18 levels in the vertical is nested within the global model, which has triangular truncation at wavenumber 42 (approximately 2.8° lat) and 18 levels in the vertical. 2) The regional model with horizontal resolution $20 \text{ km} \times 20 \text{ km}$ (covering the region 13° – 3°S , 44° – 34°W) is further nested within the first nest domain. The perturbation produced by the RSM is largely compressed in the lateral buffer zone; thus the RSM outputs in the lateral buffer zone are not used in our analysis.

In the RSM, the surface physics calculations were performed using a two-layer soil model of Pan and Mahrt (1987). The soil model is designed to describe the role of vegetation and interactive soil moisture in modifying the surface–atmosphere exchanges of momentum, energy, and water vapor. The vegetation type is mainly savanna over Nordeste and subtropical regions, and tropical forest over the Amazon basin. However, only one vegetation type can be specified in the soil model. Both savanna and forest over the whole domain were tested. With the specification of forest, the model not only overestimated the rainfall amount but also failed to capture the observed rainfall patterns over Nordeste. With the specification of savanna, the model produced rainfall reasonably well over Nordeste (see next section), although it underestimated rainfall in the Amazon basin, which is consistent with the Amazon deforestation study by Shukla et al. (1990). This may imply that the effects of misrepresentation of vegetation over the Amazon basin in the model are mainly over the Amazon basin, and

the impacts over Nordeste are small. Since Nordeste is our region of interest, we chose savanna over the whole domain in our study. Soil moisture and soil temperature are initialized by ECHAM3's inputs.

Large-scale forcing for the regional forecast experiment was obtained from 10 AGCM forecast runs, each integrated for 8 months from distinct initial conditions in December 1998. Three AGCM runs were chosen to span the possible range of outcomes from the glo-

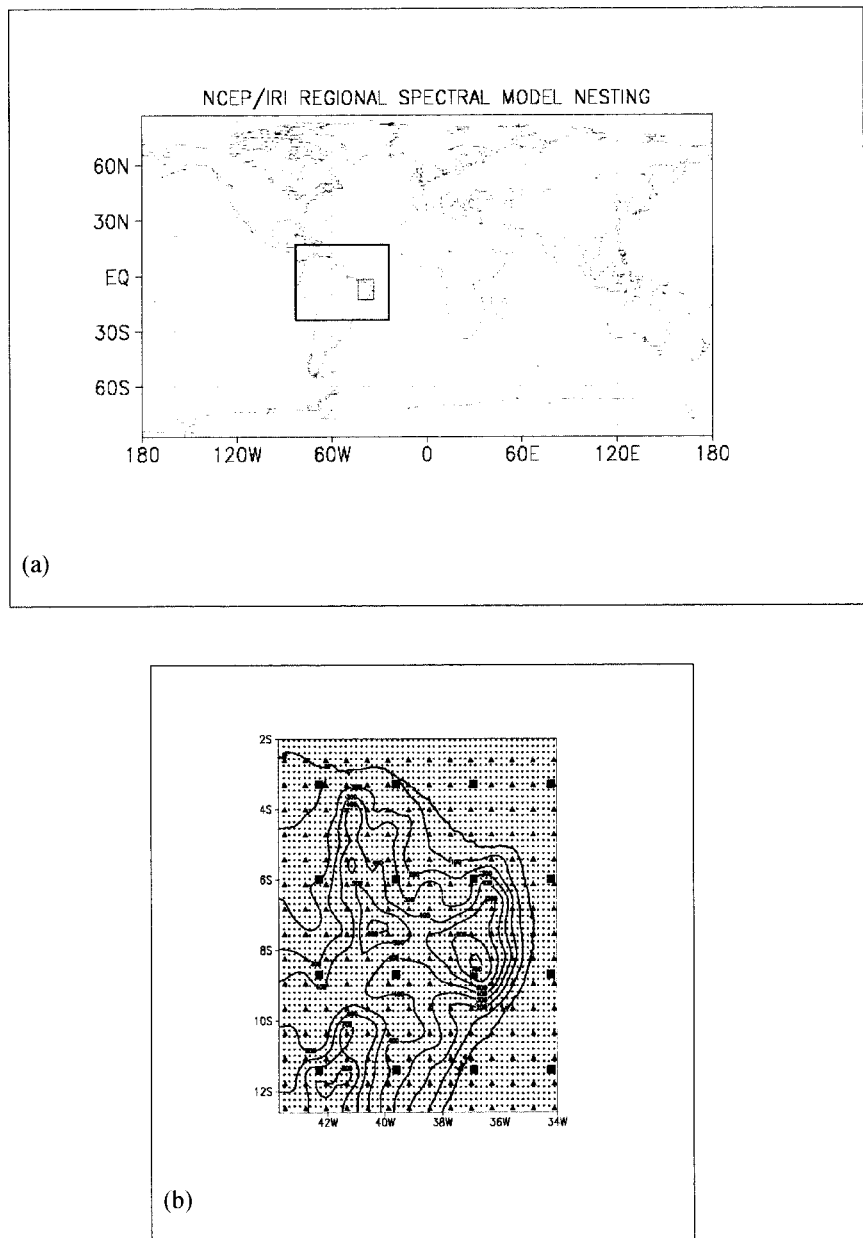


FIG. 1. (a) Schematic representation of the global and regional models' spatial domains. (b) Topography (m) used with RSM-20 model and the horizontal resolutions for the ECHAM3 (full squares), RSM-80 (full triangles), and RSM-20 (dots) horizontal "grids." Contour interval for topography is 100 m.

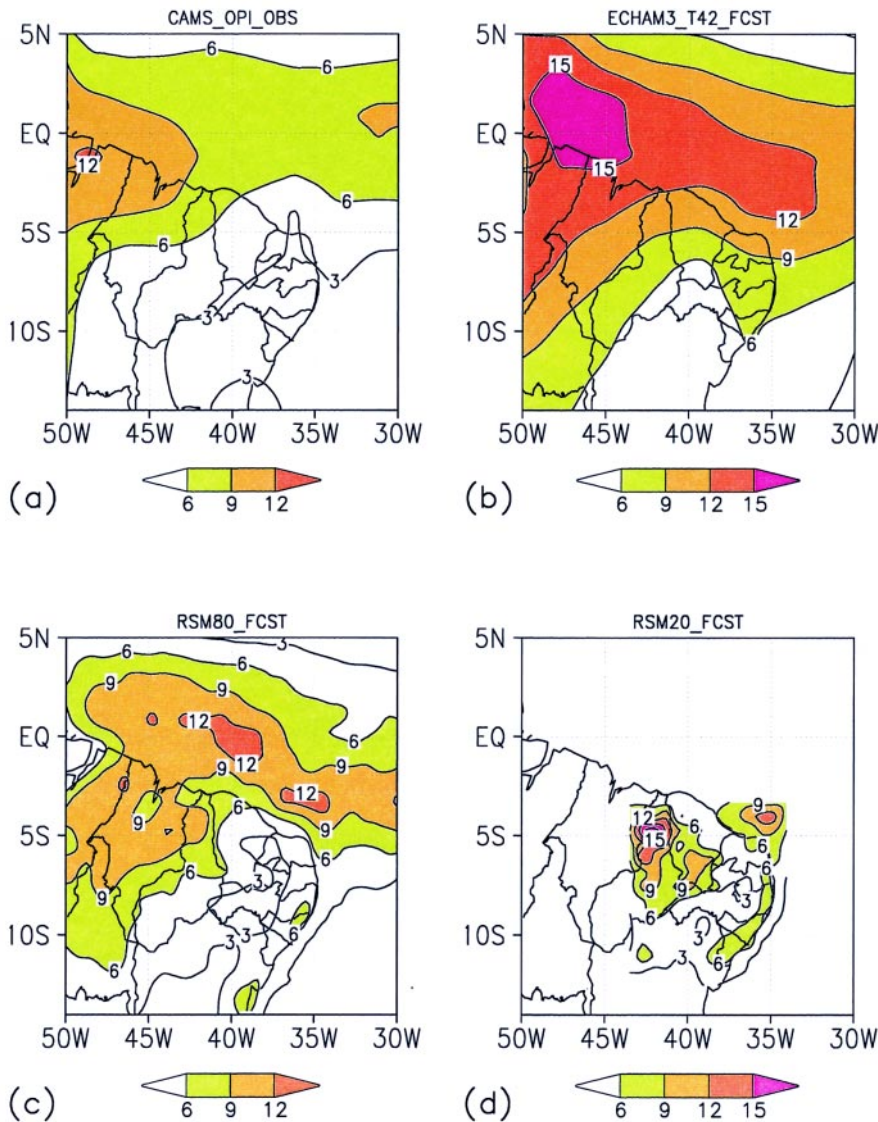


FIG. 2. Jan–Apr 1999 rainfall totals over Nordeste (in mm day^{-1}) for (a) CAMS_OPI (OLR Precipitation Index) observations, (b) ECHAM3 forecast, (c) RSM-80 forecast, and (d) RSM-20 forecast. Contour interval is 3 mm day^{-1} . Contours greater than 6 mm day^{-1} are shaded.

bal model. Each of the three RSM-80 nested forecast experiment outputs were then used to force the RSM-20 runs. The large-scale information of zonal and meridional components of the wind, specific humidity, temperature, and surface pressure are updated every 6 h and are taken from the larger domain's model outputs. Global SST forecast values were obtained by blending NCEP's coupled model SST forecasts for the tropical Pacific (Ji et al. 1994) with Centro de Previsão de Tempo e Estudos Climáticos's (CPTEC) statistical SST forecast for the tropical Atlantic (Repelli and Nobre 2001), IRI's statistical SST forecast for the Indian Ocean (Mason et al. 1999), and

damping the most recent 1-month-mean observed SST anomalies in the extratropics.

Monthly rainfall data used for verification were NCEP Climate Anomaly Monitoring System (CAMS)—a blend of rain gauge data over the continents and satellite estimates over the ocean (Janowiak and Xie 1999)—and rain gauge data over Brazil from Instituto Nacional de Meteorologia.

3. Results

Figure 2 shows the January–April 1999 observed rainfall, ensemble mean forecast rainfall for ECHAM3, RSM-80 over Nordeste and part of the Atlantic Ocean, and RSM-20 over the Nordeste. ECHAM3's forecast (Fig. 2b) resembles the observations (Fig. 2a) but overestimates rainfall amounts everywhere. In particular, the rainfall band over the equatorial region and Nordeste was too wide relative to observations. This resulted in a large positive rainfall bias over the northern part of Nordeste. The RSM-80 forecast (Fig. 2c), on the other hand, shows a spatial pattern that resembles those of ECHAM3 and observations, but with reduced positive bias relative to the global model forecast. Yet, both ECHAM3 and RSM-80 forecast the maxima rainfall band along the equator [here identified with the Atlantic intertropical convergence zone (ITCZ)] displaced southward of observations. The rainfall pattern forecast by RSM-20 shown in Fig. 2d also overestimated observations, principally along the eastern coast and the interior mountain range. In both RSM-80 and RSM-20 runs, the same physics schemes are used. The cumulus convection parameterization scheme can show a significant sensitivity to horizontal resolution (Giorgi and Marinucci 1996), and thus can present quite different behaviors in the nested models. The

model results suggest that RSM-80 can produce the rainfall patterns reasonably well, while the cumulus convection parameterization (i.e., Kuo scheme in RSM) should be optimized for the RSM-20.

The narrower ITCZ forecast by RSM-80 is shown in Fig. 3, which depicts the latitude–time cross sections of rainfall averaged over the longitude band 40°–36°W for observations, and RSM-80 and ECHAM3 forecasts. While rainfall rates greater than 8 mm day⁻¹ barely cross 2°S for the observations shown in Fig. 3a, the 8 mm day⁻¹ contour reaches 4°S for the RSM-80 (Fig. 3b) and south of 6°S for the ECHAM3 (Fig. 3c). Accordingly, the southernmost migration of the observed rainfall maximum shown in Fig. 3a (thick continuous line labeled “0”) barely reaches the equator, while each of the RSM-80 and ECHAM3 rainfall maxima reach 2°S (Fig. 3b) and 4°S (Fig. 3c), respectively. The results shown in Figs. 2 and 3 suggest that both the forecasts of broader ITCZ and its southward displacement explain in part the positive rainfall biases forecast over the Nordeste (figure not shown).

While the analysis of seasonal biases may represent a first estimate of the model errors, they do not reveal possible discrepancies between the temporal distribution of forecast and observed rainfall within the season. For that end, the root-mean-square error (rmse) of the monthly data was calculated using rain gauge data over the Nordeste (Fig. 4).

From the standpoint of rmse, Fig. 4 clearly shows that RSM-80 generated the best seasonal forecast among the three. The rmse for ECHAM3 over Nordeste is in part due to the unrealistically wide ITCZ forecast by the global model. One possible cause for the lower rmse associated with RSM-80 is the narrower ITCZ it generates, as inferred from Fig. 3. However, the general improvement along the coast is an indication that surface processes may also be contributing to the better performance of the regional model. The spatial pattern of the rmse gener-

ated by RSM-20 (Fig. 4c) strongly projects onto the local orography (shown in Fig. 1b), suggesting that orographical effects are contributing to the excessive rainfall forecast by RSM-20 over the mountain ranges. This again reveals the need to modify the convection scheme used by the regional model at the 20-km grid resolution, to correct for the excess rainfall produced in the presence of higher values of topography. The band of positive rainfall bias along the eastern shore of Nordeste could also be due to spurious low-level convergence induced by the mismatch of surface friction in the initial surface winds from the ECHAM to

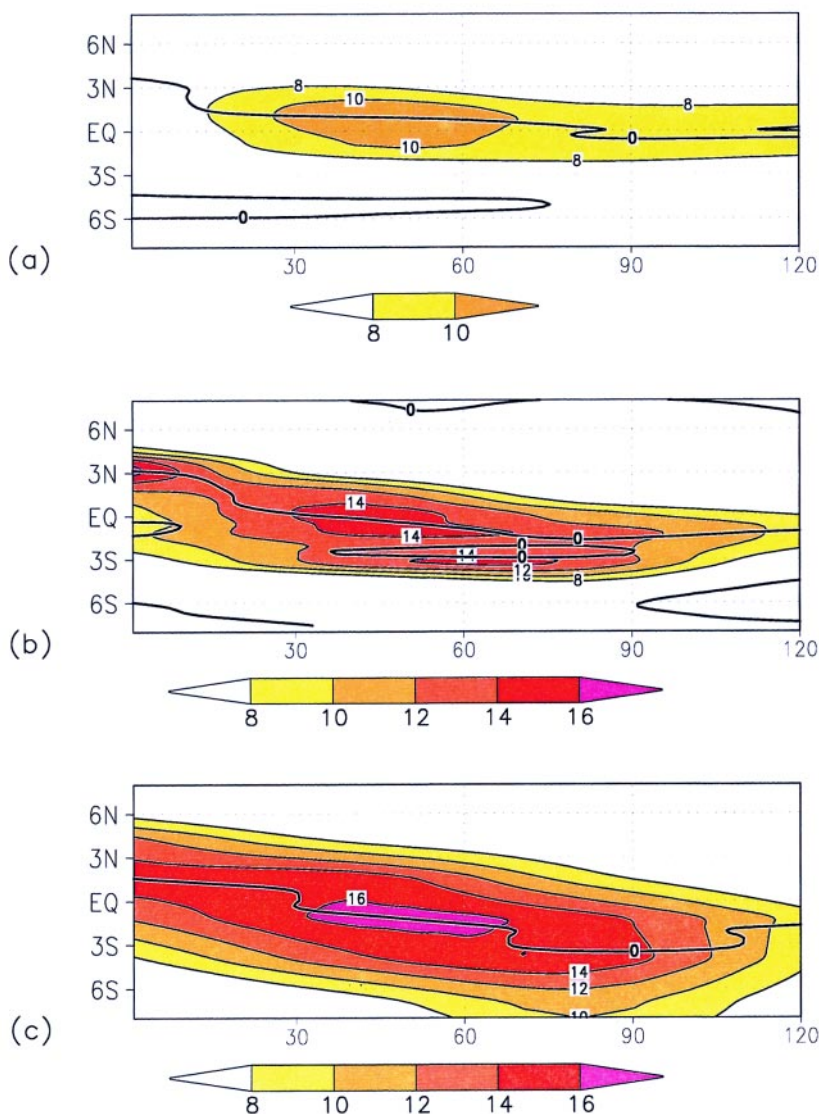


FIG. 3. Latitude–time (days) cross section of monthly rainfall averaged for the longitude band 40°–36°W for (a) CAMS_OPI observations, and (b) RSM-80 and (c) ECHAM3 ensemble mean forecasts. Contour interval 2 mm day⁻¹. The thick lines labeled 0 represent the positions of the rainfall maximum. Contours greater than 8 mm day⁻¹ are shaded. Latitudes (degrees) are shown in the y axis, time (days) in the x axis.

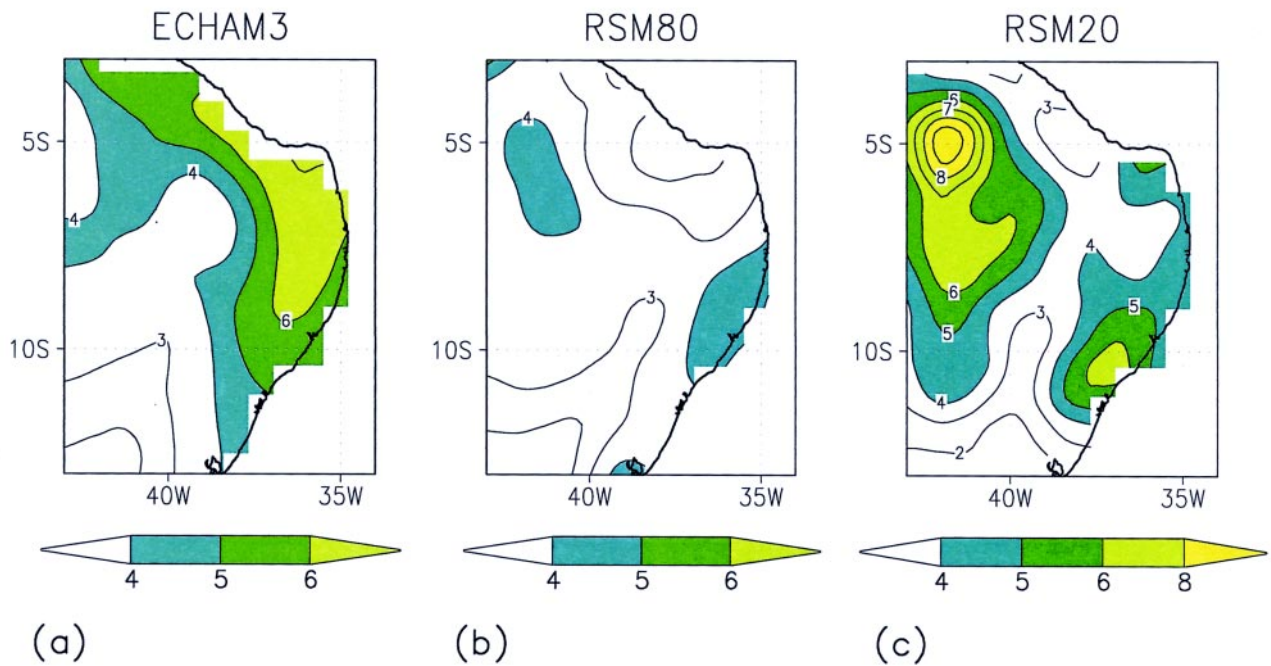


FIG. 4. Root-mean-square error between observed monthly rain gauge data and (a) ECHAM3, (b) RSM-80, and (c) RSM-20 ensemble mean monthly forecasts for the period Jan–Apr 1999 over Nordeste. Contour interval is 1 mm day⁻¹; contour values greater than 4 mm day⁻¹ are shaded.

the 80- and 20-km grid resolution models. In addition, it will be necessary to refine the types of soil and vegetation for the region at comparable resolution. It is noteworthy, also, that the spatial pattern of the rmse field for RSM-80 (Fig. 4b) resembles that for RSM-20 (Fig. 4c), but with magnitudes halved. Therefore, it is reasonable to assume that the RSM-80 rmse field is, in part, caused by topographic effect on the model's precipitation. The fact that RSM-20 nesting amplified RSM-80 systematic forecast errors over the mountain ranges in Nordeste suggests that surface processes do impact the seasonal rainfall forecast in the regional model. It indicates also that the convection scheme used in RSM-20 must be adjusted to the higher values of topography.

Although the spatial anomaly correlations between each of the forecasts and observation (station data interpolated to the models' grid) over the Nordeste are modest, again the RSM-80 showed the best result. The correlations are ECHAM3: 0.26; RSM80: 0.41; RSM20: 0.23.

In the analyses of model performance, it is also of interest to analyze the temporal variability of area averages. To this end, 5-day running means of daily rainfall averaged over the Nordeste (11.5°–3.5°S, 43.5°–35.5°W) were computed and are shown in Fig. 5 for observations (vertical bars) and each model

ensemble mean forecasts (thick continuous line). Also shown in Fig. 5 are the area averages of each member forecast (thinner dashed lines). While both versions of the regional model present smaller rmse, bias, and intermember ensemble spread than the global model, RSM-80 (Fig. 5b) stands out as the best overall forecast for this experiment, with the least rmse and bias (Table 1), as well as the smallest intermember spread. ECHAM3 (Fig. 5a) shows the largest rmse and bias (7.0 mm against the observation's 3.5 mm), also showing the largest spread of predictions among all models. Yet, it is interesting to observe in Fig. 5 the similarity among the temporal variability of the global and regional models' ensemble means, suggesting that the regional model area-averaged forecasts depend on the temporal variability of the global model forcing. This indicates that while the nesting process used in this work can improve the global model's forecast, much of the basic character of the temporal variability of area-averaged rainfall remains tied to the global model's forecast. Yet, there seems to be some mesoscale precipitation activity, which is forecast only by the regional models.

One new development that unfolds from the suggestion that the intraseasonal variability of both observed and forecast time series over the Nordeste is comparable (Fig. 5) is the possibility that the higher

statistical moments of the rainfall distribution over the region are, to a certain extent, predictable. One such statistic is the temporal variance of rainfall about the mean (which already may indicate an anomaly) rainfall forecast over a certain area, which can be translated into shifts of the distribution of probability for the occurrence of dry spells or heavy rainfall periods over that area. These kinds of information have direct economic and social impacts on activities such as agriculture, water resources, and civil defense.

Figure 6 shows the probability density function (pdf) for observations and each of the models forecast over the same area used for computing Fig. 5. It was calculated by stratifying the area-averaged daily rainfall into 10 classes for the 4 months of the forecast experiment. The x axis in Fig. 6 shows the rainfall classes and the y axis the number of days per month that the area-averaged rainfall for the area of study fell into each class. The pdf curve for observations in Fig. 6 shows a characteristic gamma-shaped distribution, with maximum frequency of $1\text{--}5\text{ mm day}^{-1}$. It is noteworthy that although the ECHAM3 and RSM-20 show a tendency toward a bimodal pdf distribution, RSM-80's pdf does not, and most resembles that of the observations. It shows the maximum frequency in the same class as that of observations (at the $1\text{--}5\text{ mm day}^{-1}$ class) and is essentially devoid of a secondary anomalous peak in the $7\text{--}11\text{ mm day}^{-1}$ class. The RSM-20's pdf also shows the most likely rainfall rate at $1\text{--}5\text{ mm day}^{-1}$, but its secondary peak at $7\text{--}11\text{ mm day}^{-1}$ is the most pronounced among the forecasts. This feature of the RSM-20 forecasts is linked to the heavy rainfall to-

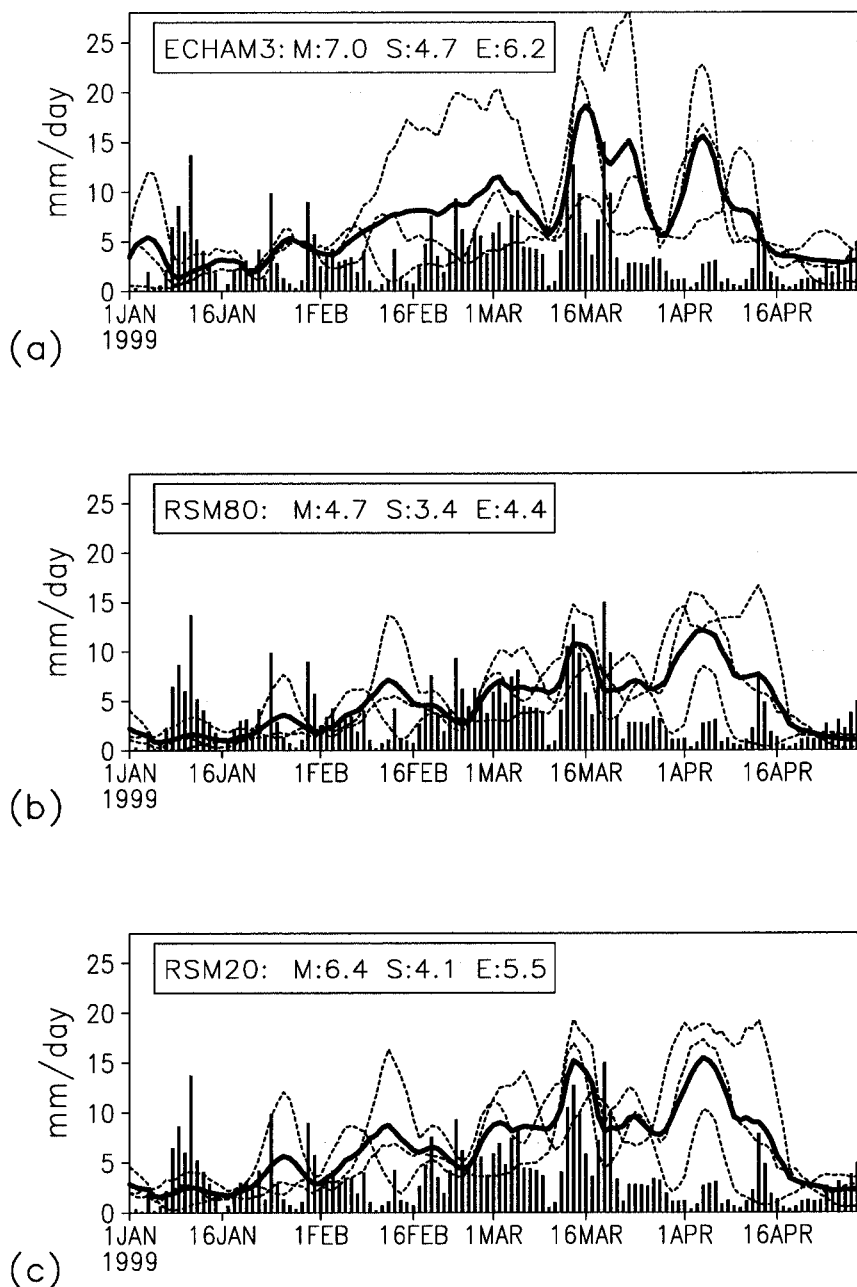


FIG. 5. Five-day running means of daily rainfall averaged over the Nordeste ($11.5^{\circ}\text{--}3.5^{\circ}\text{S}$, $44.5^{\circ}\text{--}35.5^{\circ}\text{W}$) for (a) ECHAM3, (b) RSM-80, and (c) RSM-20 ensemble mean forecasts (thick continuous line) and the forecast of each ensemble member (thin dotted lines). Observations are shown in all three panels as vertical bars. The mean (M), std dev (S), and rmse (E) for each model's forecast are indicated in the upper-left corner of the graph (in mm day^{-1}). The x axes show the dates and y axes show the rainfall (scaled in mm day^{-1}).

totals along topographic elevations shown in Fig. 2c. The ECHAM3 forecasts also shows a bimodal, but less pronounced, pdf profile, with the maximum rainfall class at $3\text{--}7\text{ mm day}^{-1}$. It is evident from the analysis of Fig. 6 that in terms of distribution, the RSM-80 also generated the best results, suggesting the possibility

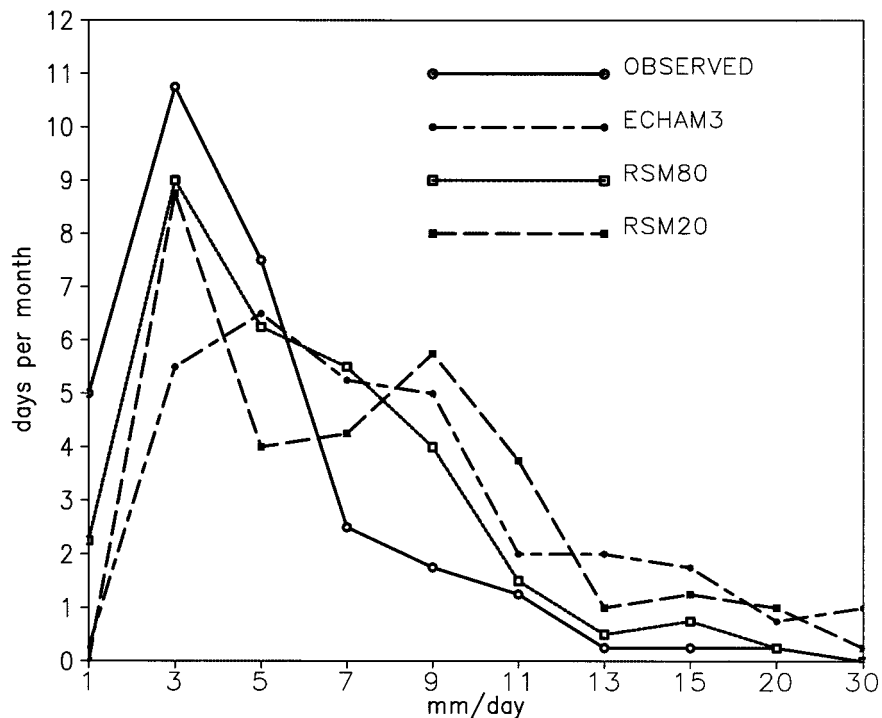


FIG. 6. Probability density function of the number of days per months (y axis) vs classes (in mm day^{-1}) (x axis) of area-averaged daily rainfall over the Nordeste (11.5° – 3.5° S, 44.5° – 35.5° W) for the whole period of the experiment (Jan–Apr 1999). Observed, and forecast by ECHAM3, RSM-80, and RSM-20 are as shown by legend in the upper-right corner.

fall per calendar month for the RSM-80 ensemble forecasts (Figs. 7b,d,f) and observations (Figs. 7a,c,e) over the portion of Brazil within the computational domain of RSM-80. The overall distribution of the areas with high and low number of days without rainfall as forecast by the RSM-80 shows good resemblance with that observed. The larger discrepancies are apparent over the mouth of the Amazon River and the southern boundary of the domain. Similarly, the spatial distributions of the number of days with light, moderate, and heavy rainfall (figures not shown) depicted good agreement with observations, even though the forecast numbers of days with moderate rainfall are generally larger than observed. This is in agreement with the positive error for the 7–11 mm day^{-1} rainfall class shown in Fig. 6 for

that higher-order statistics of the weather can be predicted over some regions.

Another view of the analysis of weather variability statistics in seasonal timescales can be shown by the spatial distribution of the number of days within rainfall classes (e.g., without/light/moderate/heavy rainfall) per calendar month. Figure 7 shows the spatial distribution of the number of days without rain-

all the models' forecasts. The spatial patterns of days with light, moderate, heavy, or without rainfall (figures not shown) for ECHAM3 did not compare well with observations, in great part due to the large positive biases of the ECHAM3 rainfall forecast (e.g., Fig. 2b and Fig. 6). This is one more aspect where the regional model at 80-km resolution has shown a definitive improvement over the global model forecasts.

TABLE 1. Mean, std dev, and rmse (in mm day^{-1}) for the area-averaged time series of the rainfall ensemble mean forecasts over the Nordeste for ECHAM3, RSM-80, and RSM-20 for the period 1 Jan–30 Apr 1999; and the mean and std dev for observed rainfall over the same area and period.

	Mean	Std dev	Rmse
ECHAM3	7.0	4.7	6.2
RSM-80	4.7	3.4	4.4
RSM-20	6.4	4.1	5.5
Observed	3.5	3.0	—

4. Conclusions

The IRI dynamical downscaling suite of atmospheric models (ECHAM3 plus RSM) was used to generate forecasts for the 1999 rainy season over northeast Brazil (Nordeste). The case shown suggests that the nesting strategy used was able to generate rainfall forecasts that were in closer agreement with observations, and better than the global model forecasts. The regional model at 80-km horizontal resolution generated the best forecasts, improving the global model's forecasts in terms of the bias, mean square error, and interensemble spread. The regional model at 20-km resolution also presented a smaller

spread among the ensemble members; however, it enlarged the systematic errors present in the driving 80-km model. It is suggested that finer tuning of the surface processes and the convection scheme used in the regional model is necessary at the 20-km resolution.

One of the main results of this study is the indication that regional models can be used to forecast the statistics of the weather phenomena within the rainy season of Nordeste. These statistics include both the probability distribution of area-averaged daily rainfall and the spatial patterns of the frequency and duration of dry spells or heavy precipitation periods. Such statistics, derived from the regional model, if proven to be predictable as the present study suggests, are to become important forecast tools in assisting decision makers on a large spectrum of human activities.

It is unclear at this point, however, whether the better forecasts generated by the regional model were due to the increase in the model's horizontal resolution and/or, more specifically, its more accurate representation of topographically induced physical processes, among the many possibilities. One of the reasons for better seasonal rainfall forecasts generated by the regional model first nesting (i.e., the 80-km grid), compared to the global model's forecast, is its better-defined Atlantic ITCZ structure. The 20-km grid nesting generated seasonal rainfall forecasts with large positive bias over the mountain ranges within the model's domain, suggesting the need to tune the convection scheme and surface parameters used. Results of another study of dynamical downscaling over eastern Africa, using the same methodology (Sun and Graham 2001, manuscript submitted to *J. Geophys. Res.*), indicated that the nested suite of models could better

simulate topographically induced seasonal rainfall. However, a complete in-depth study needs to be done to access the statistical significance and the source of improvements of the results as presented in this forecast exercise.

Acknowledgments. The authors acknowledge discussions with Dr. N. Graham, the valuable comments of the anonymous reviewers, and suggestions for improvements made by Drs. Tony Barnston and Steve Zebiak. This work was done at the IRI, which is supported by a NOAA/OGP grant and Columbia University. The first author acknowledges support from CPTEC/INPE in Brazil.

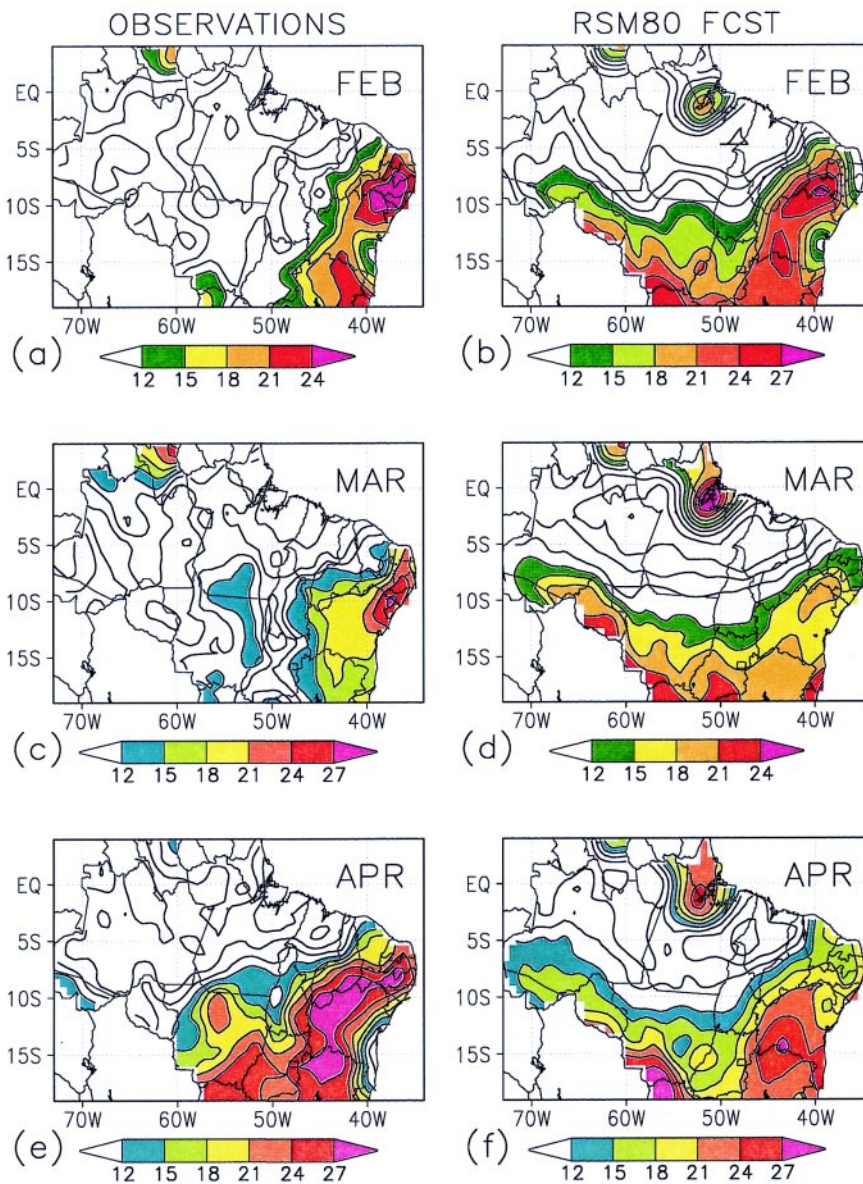


FIG. 7. Number of days without rainfall over northern Brazil for Feb, Mar, and Apr 1999. Left column: observations; right column: RSM-80 forecast. Contour interval is 3 days. Contours greater than 12 days are shaded.

References

- Fennessy, M. J., and J. Shukla, 1998: Seasonal prediction experiments with a regional model nested in a global model. Center for Ocean–Land–Atmosphere Studies Rep. 63, 34 pp.
- Galvão, C. O., R. T. Clarke, T. D. Davies, and P. D. Jones, 1999: Evaluation of seasonal forecasting methods for water resource management in northeastern Brazil. *Hydrological Extremes: Understanding, Predicting, Mitigating*, Lars Gottschalk, Ed., International Association of Hydrological Sciences Press, 289–295.
- Giorgi, F., and M. R. Marinucci, 1996: An investigation of the sensitivity of simulated precipitation to model resolution and its implications for climate studies. *Mon. Wea. Rev.*, **124**, 148–166.
- Janowiak, J., and P. Xie, 1999: CAMS–OPI: A global satellite-rain gauge merged product for real-time precipitation monitoring applications. *J. Climate*, **12**, 3335–3342.
- Ji, M., A. Kumar, and A. Leetmaa, 1994: A multiseason climate forecast system at the National Meteorological Center. *Bull. Amer. Meteor. Soc.*, **75**, 569–578.
- Ji, Y., and A. D. Vernekar, 1997: Simulation of the Asian summer monsoons of 1987 and 1988 with regional model nested in a global GCM. *J. Climate*, **10**, 1965–1979.
- Juang, H.-M. H., and M. Kanamitsu, 1994: The NMC nested regional spectral model. *Mon. Wea. Rev.*, **122**, 3–26.
- Kirtman, B. P., Ed., 1999: *Experimental Long-Lead Forecast Bulletin*. Center for Ocean–Land–Atmosphere Studies, 87 pp. [Available from COLA, 4041 Powder Mill Rd., Suite 302, Calverton, MD 20705-3106.]
- Leung, L. R., A. F. Hamlet, D. R. Lettenmaier, and A. Kumar, 1999: Simulations of the ENSO hydroclimate signals in the Pacific Northwest Columbia River basin. *Bull. Amer. Meteor. Soc.*, **80**, 2313–2329.
- Mason, S. J., L. Goddard, N. E. Graham, E. Yulaeva, L. Sun, and P. A. Arkin, 1999: The IRI seasonal climate prediction system and the 1997/98 El Niño event. *Bull. Amer. Meteor. Soc.*, **80**, 1853–1873.
- Mechoso, C. R., S. W. Lyons, and J. A. Spahr, 1990: The impact of sea surface temperature anomalies on the rainfall over northeast Brazil. *J. Climate*, **3**, 812–826.
- Pan, H.-L., and L. Mahrt, 1987: Interaction between soil hydrology and boundary layer development. *Bound.-Layer Meteor.*, **38**, 185–202.
- Repelli, C. A., and P. Nobre, 2001: Statistical prediction of sea surface temperature over the tropical Atlantic. *Int. J. Climatol.*, in press.
- Shukla, J., 1981: Dynamical predictability of monthly means. *J. Atmos. Sci.*, **38**, 2547–2572.
- , C. A. Nobre, and P. Sellers, 1990: Amazon deforestation and climate change. *Science*, **247**, 1322–1325.
- Sun, L., and N. Graham, 2001: Climate simulation over East Africa using the NCEP Regional Spectral Model. *J. Geophys. Res.*, in press.
- Ward, M. N., and C. K. Folland, 1991: Prediction of seasonal rainfall in the north nordeste of Brazil using eigenactors of sea-surface temperature. *Int. J. Climatol.*, **11**, 711–743.
- Zebiak, S. E., and M. A. Cane, 1987: A model El Niño–Southern Oscillation. *Mon. Wea. Rev.*, **115**, 2262–2278.

Call for Weather-Related Art and Photos

The *Bulletin of the American Meteorological Society* invites submission of original, weather-related art and photos for potential publication in future issues of the magazine. The *Bulletin* staff is especially interested in work that is artistic and creative, featuring a unique, interesting perspective; chosen works will be used to help add more graphic appeal to the *Bulletin*. Specific use of the images will be determined by the production staff. Please be aware that your submission will not be peer reviewed—we will be looking at submissions more from an aesthetic viewpoint than a scientific one. (Photos intended for scientific publication should be submitted following normal *Bulletin* guidelines for peer-reviewed submissions.) Nonetheless, all submissions will be given equal consideration.

We hope that you will take this ongoing opportunity to inspire your colleagues and shape the look of your Society's publication. Ownership of the works will be retained by the artist/photographer; we do not offer payment for published submissions.

Submission requirements: For artwork, please do not submit the original work of art—send only a high-quality color photo of the piece. For art and all other photographs submitted for consideration, send only first-quality, camera-ready prints or slides (no photocopies, please). Submissions will not be returned unless accompanied by a self-addressed envelope with correct postage.

Please include with the submission your name, the title of the work (if applicable), and any other relevant information. If a description of the submission would be helpful, please include a succinct caption.

Please submit your work to: David Gershman, Manager of Art and Design, AMS, 45 Beacon St., Boston, MA 02108-3693.